Analytical Approach of the Arching Dual Effect Describing the Stability of Slurry-Wall Trenches in Cohesionless Soil

Riadh Saadi[1]; Mohamed Baheddi, Ph.D.[2]; and Noureddine Ferhoune, Ph.D.[3]

Abstract: Stability of slurry trenches is an important issue during the construction of groundwater cutoff and diaphragm walls and, thus, has gradually drawn additional attention. With the aim of controlling the stability and collapse mechanism of slurry walls better, an analytical approach based on interactions between horizontal and vertical arching effects was conducted to estimate the stability factors for general and local stability of a slurry-supported trench panel in cohesionless soils. The results show that arching has certain characteristics that affect soil behavior near the trench, including directions of loading and unloading of soil, variation of active pressure coefficient on the sidewall interface, and a created downward load transfer mechanism. The trench stability depends on two types of safety factors; the first factor prevents sliding collapse (overall stability), and the second factor prevents collapse of the soil interface (local stability) because local interface instability triggers overall trench collapse in cohesionless soil. The solution was compared with field measurements and three-dimensional (3D) finite-element analyses (with the effect of the third dimension), which permitted study of the influence of the arch located in the third direction. The satisfactory correspondence validates this approach and shows that the 3D analytical analysis perfectly describes the phenomenon. **DOI: 10.1061/(ASCE)GM.1943-5622.0000973.** © *2017 American Society of Civil Engineers.*

Author keywords: Deep trench; Arching effect; Diaphragm wall; Slurry trench; Flat excavation.

Introduction

Slurry trenches are used in the construction of groundwater cutoff walls and subsurface structural diaphragm walls. The stability of slurry trenches has attracted great attention among geotechnical researchers and the industry as a whole because instability of the slurry trench is common in underground engineering. The safety factor is an important index in the design of the slurry trench (Mohamed 2015; Piaskowski and Kowalewski 1965), but little research has been carried out on the theoretical explanation for the importance of slurry trench stability. The holding of the small-diameter circular cavity trench is easily explained by the formation of an annular compression vault. However, the holding of a flat, deep excavation filled with benthonic mud (slurry wall) in cohesionless soil cannot be attributed to the same explanation because stress rearrangements will take place on elliptic surfaces far from the flat lateral surface of the trench, unlike trenches of annular shape in which the stress paths take the lateral surface of the trench as the vault.

Using several theories developed by geotechnical researchers, several attempts have been made to explain the stability of trenches filled with mud. Different methods adopted to deal with this problem have been classified into the following types: theoretical methods, namely the *limit-equilibrium method* (Fox 2004) and *limit analysis* (Xiao et al. 2015); numerical analyses, such as *finite-element modeling* (Carlos and Theodoros 2012) and *finite-differences modeling* (Xiao et al. 2015); and laboratory tests and field measurements. All these methods have limitations, but they have contributed to various degrees to the understanding of the performance of deep excavations.

Most of the existing studies focus on ground movements and stress paths induced by diaphragm-wall construction. Tsai presented an analytical method to evaluate the stability of weak sublayers against lateral extrusion in a slurry supported trench (Tsai 1997). Fox (2004) presented Coulomb-type force equilibrium analyses for the general three-dimensional (3D) stability of a slurry-supported trench. Yonggang et al. (2011) studied the influence factors of the stability of slurry trench sides during diaphragm wall building in soft soil by analyzing the fullness coefficient of slurry trenches corresponding to different controlling parameters. On the basis of the upper-bound limit analysis theorem, Han et al. (2013) developed two-dimensional (2D) and 3D analyses of slurry trench for local and overall stability for cohesive soil. Ng and Yan (1999) confirmed the horizontal arching and downward load transfer mechanisms during diaphragm wall installation using the finite-difference method. Gourvenec and Powrie (1999) investigated the impact of 3D effects and panel length on horizontal ground movements and changes in lateral stress during sequential installation of a number of diaphragm wall panels. Lei et al. (2014) proposed an approximate analytical solution to predict ground surface settlements along the centerline perpendicular to a slurry-supported diaphragm wall panel.

This paper presents a new analytical approach to trench stability using the limit-equilibrium method considering the contribution of the interaction between the horizontal vault and vertical arching effects during excavation in cohesionless soil. This method was developed in the worst environment for excavation; the soil was without cohesion and the water table level was at the ground surface. The aim was to assess the safety factor for general and local stability in these extreme conditions (Lei et al. 1999). For this reason, an explicit 3D analytical solution was derived in this work as a first approximation for calculating earth pressures acting on sidewalls while showing the role and influence of each arch effect on soil behavior near the trench panel

[1]Ph.D. Student, Civil Engineering, Univ. of Batna, Batna 04200, Algeria (corresponding author). E-mail: saadiriadh0202@gmail.com

[2]Professor, Civil Engineering, Univ. of Batna, Batna 04200, Algeria. E-mail: baheddi_md@yahoo.fr

[3]Professor, Civil Engineering, Univ. of Larbi Ben M'hidi Oum El Bouaghi, Oum El Bouaghi 04000, Algeria. E-mail: ferhoune.noureddine@gmail.com

Note. This manuscript was submitted on September 16, 2016; approved on March 29, 2017; published online on July 19, 2017. Discussion period open until December 19, 2017; separate discussions must be submitted for individual papers. This paper is part of the ***International Journal of Geomechanics***, © ASCE, ISSN 1532-3641.

(Tsai 1997). The validity of the solution was verified by 3D finite-element (FE) analyses. The ease of use of the formula was illustrated by comparing the calculated results with some reported field data for slurry-supported trench excavations in the Kowloon, Hong Kong, region by which the validity of the solution was also verified.

Solutions

Assumptions for the Analytical Study

The approach taken in this paper takes into account the effects of both vertical and horizontal vaults as they interact. In fact, the presence of two stress transfer mechanisms, namely, horizontal arching and downward load transfer governed by the vertical arching effect during diaphragm wall installation, was confirmed. These two mechanisms act simultaneously and result in an average reduction of horizontal stress directly behind the wall (Xiao et al. 2015). Moreover, the trench collapse occurs in two cases: unloading that does not cause a limited equilibrium state (meaning that the ground near excavation undergoes acceptable deformation) and local failure mechanisms. In the first case, collapses are triggered by the interface instability (this phenomenon is predominant in soils that have significant cohesion values) (local stability) (Lei et al. 2014). In the second case, soil relaxation causes unacceptable deformation, which leads to a limited equilibrium state in the ground, for this critical state, and the trench collapse is produced by both the overall and interface instabilities (this case is predominant in cohesionless soil) (local and overall stability) (Tsai and Chang 1996).

As explained in the previous paragraphs, local interface instability triggers overall trench collapse and vice versa in cohesionless soil, which inspired this research to deal with the second type of trench collapse. When the soil is excavated, an annular compression vault is created in the horizontal x,y-plane, releasing a block of land laterally supported by the vertical arch effect and shear forces acting on both ends of the failure wedge in the x,z-plane (Fig. 1) (Xiao et al. 2015). Arches interact in a way that gives a different slip surface (curved surface of Fig. 1). Therefore, the holding of a deep trench panel related to the soil wedge stability results from the double-arching effect. In fact, the excavation is surrounded on both sides by a detached soil wedge that must be stabilized to ensure the trench stability.

Analytical Model of Trench Excavation

The aim of this model is to show the arching effect on deep trench stability, so it was necessary to eliminate cohesion that plays a

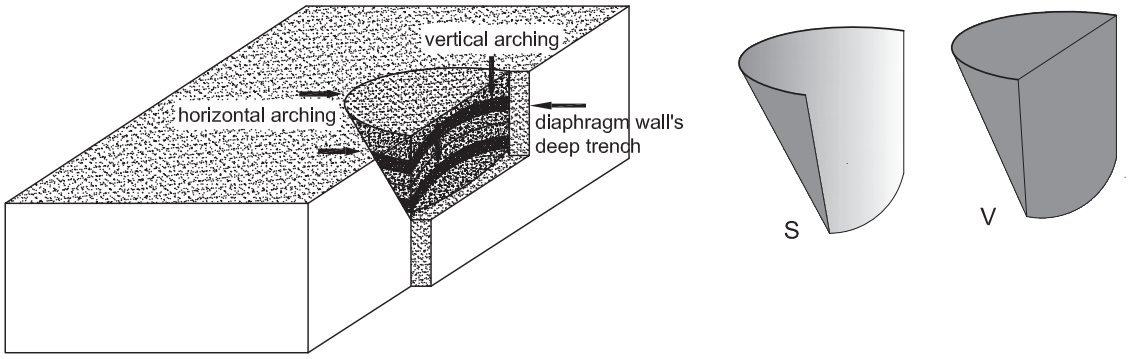

Fig. 1. Load transfer mechanisms governed by the arching dual effect creating slip surface, *S*, and corner, *V*

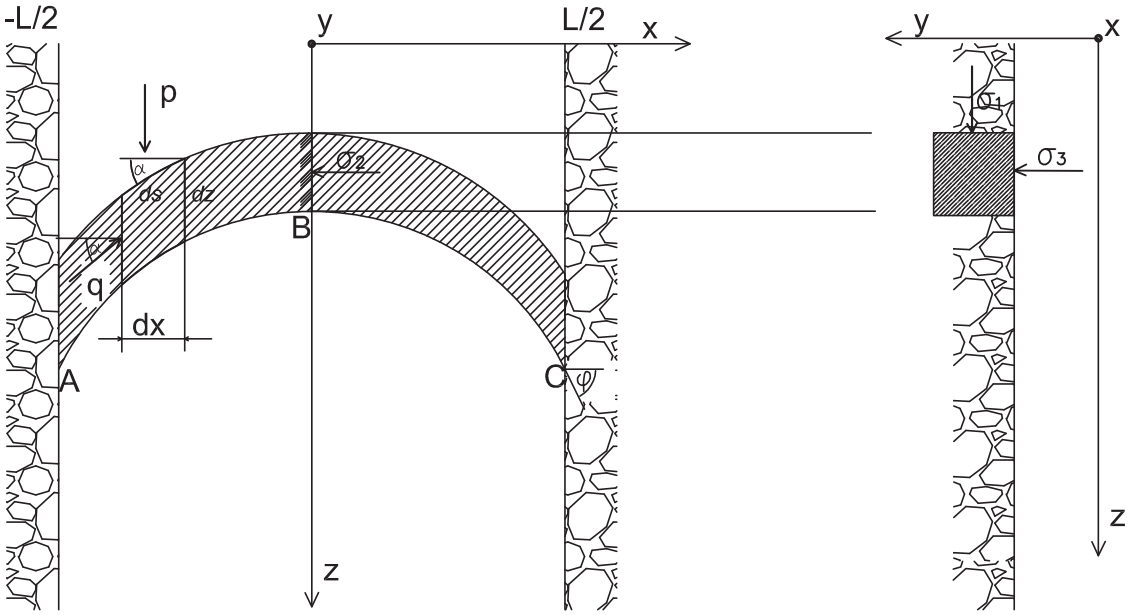

Fig. 2. Arch formed in the vicinity of the excavation limited by ABC

stabilizing role independently. However, the apparition of the arching effect in the both directions (horizontal and vertical) requires an initial deformation, which depends to stress variation related to the friction angle, water table level, and soil density in cohesionless soil (Tsai and Chang 1996). Thus, cohesionless soil ($c = 0$) with angle friction ($\varphi > 20°$) was assumed as was the water table level at the ground surface (i.e., worst conditions for trenching).

Prior to the excavation of a trench, the initial stress state of an undisturbed ground may be assumed to be in the K_0 condition, where K_0 is the coefficient of lateral earth pressure at rest. For homogeneous saturated soils, the horizontal and vertical total earth pressures at rest, P_h and P_v, at a given depth, z, below the ground surface can be expressed as

$$P_h = K_0(\gamma_{sat} - \gamma_w)z + \gamma_w z \quad (1)$$

$$P_v = \gamma_{sat} z \quad (2)$$

where γ_{sat} = saturated unit weight of soil; and γ_w = unit weight of water. A trench is of length, L, width, W, and depth, D (Fig. 2).

To describe downward load transfer mechanisms, basic formulas for the vertical functions under the influence of arching are needed. In the x,z-plane behind the excavated sidewall, stress distribution is influenced by the vertical arching effect. Specifically, the effective stress σ'_1 in the z direction and σ'_2 in the x direction are under the influence of vertical arching. The downward load transfer mechanisms stop the increase of σ'_1 toward a limit value, which generates a limit stress value of σ'_2 when the trench depth is sufficiently large.

Vertical Arching

The authors considered that arcs are formed in the vicinity of the excavation limited by ABC (Fig. 2). Under these conditions, the

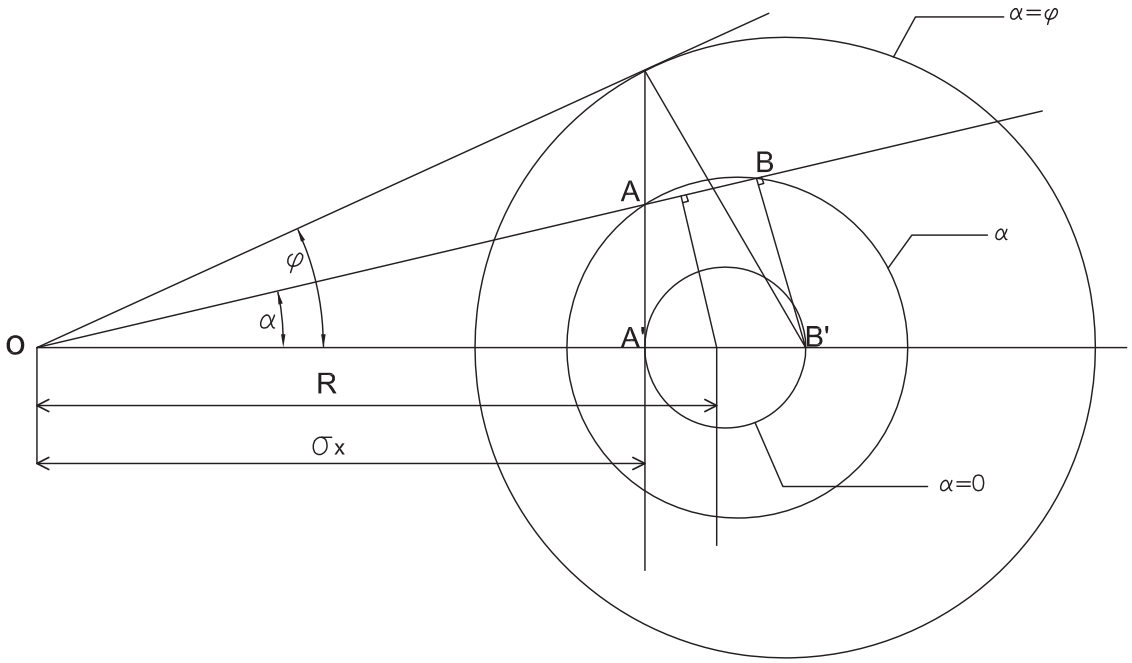

Fig. 3. Stress components acting on elementary volumes: α, $\alpha = 0$, $\alpha = \varphi$

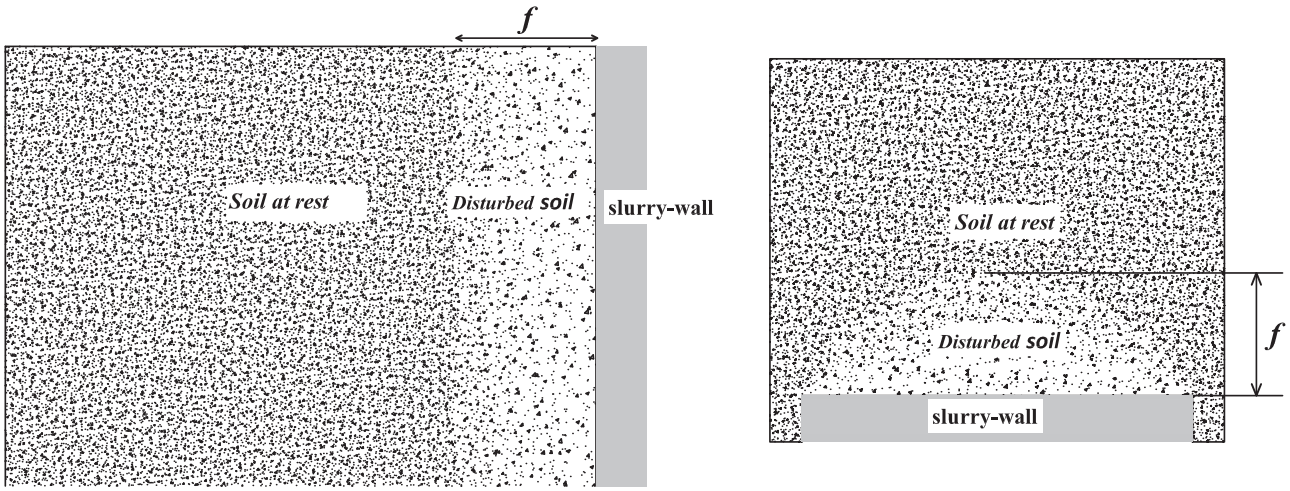

Fig. 4. Disturbed soil area near the trench under the horizontal arching influence

small elementary volume limited by the facets ds and dz undergoes q and p stresses such that q is parallel to ds and p is vertical.

It follows from the equilibrium of horizontal stresses that the normal component of q on the dz surface is constant along the arc ABC. Thus, σ_x is σ'_2 with α of 0 at the top of the arc (Point B), and shear stresses reach a maximum value, τ_A and τ_C, when α is φ at the arc ends (Points A and C) as shown (Fig. 2) and described as

$$\sigma_x = q\cos\alpha$$
$$\tau_{A,B} = q\ \sin\alpha \tag{3}$$

Furthermore, the arc was assumed to be charged uniformly on the upper surface, which means that each elementary surface ds on the arc upper surface was under constant normal stress equal to the major stress σ'_1 according to Eq. (4) as

$$\frac{p}{\cos\alpha} = \sigma'_1 = \text{constant} \tag{4}$$

The stresses acting on elementary volumes belonging to the arc $(\alpha, \alpha = 0, \alpha = \varphi)$ can be represented through Mohr's circle (Fig. 3). The components q and p are given in magnitude by the vectors OA and OB on the basis of Eqs. (3) and (4) and the schematic representation of the components; the formula for major principal stress σ'_1 is derived at the arbitrary points of

$$\frac{p+q}{2} = R\cos\alpha$$
$$\sigma'_1 = 2R - \frac{\sigma_x}{\cos\alpha^2} \tag{5}$$

Stress components acting on elementary volumes located at specific points of the arc $(\alpha, \alpha = 0, \alpha = \varphi)$ are summarized graphically in Fig. 3. On the top of the arc, α is 0, p is σ'_1, and $q = \sigma_x = \sigma'_2$, as represented by vectors OB′ and OA′. At the arc ends, α is φ; therefore, p is q, and this point represents a critical limit of the shear failure state. Arc ABC, as a whole, is subjected to five vertical forces: its own weight, $\gamma\,(L\,dz)$; the two support reactions τ_A and τ_C on the A and C ends; and the resulting elemental forces, $q\,ds$, on each side of the arc surface:

$$\int_{ABC} q\,ds = \int_{-L/2}^{+L/2} \frac{p}{\cos\alpha}\,dx = L\left(\frac{p}{\cos\alpha}\right) \tag{6}$$

The difference between the upper and lower faces is

$$L\frac{d}{dz}\left(\frac{p}{\cos\alpha}\right)dz \tag{7}$$

The arc is in the equilibrium state $\sum \mathbf{F} = 0$.

$$L\frac{d}{dz}\left(\frac{q}{\cos\alpha}\right)dz + 2\tau_A dz - \gamma\,L\,dz = 0 \tag{8}$$

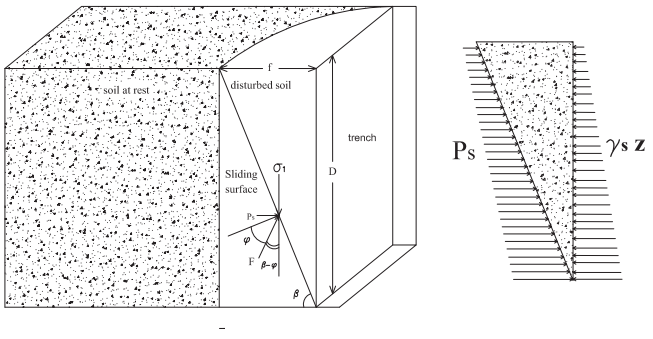

Fig. 6. Downward load interaction with horizontal arching through the sliding surface

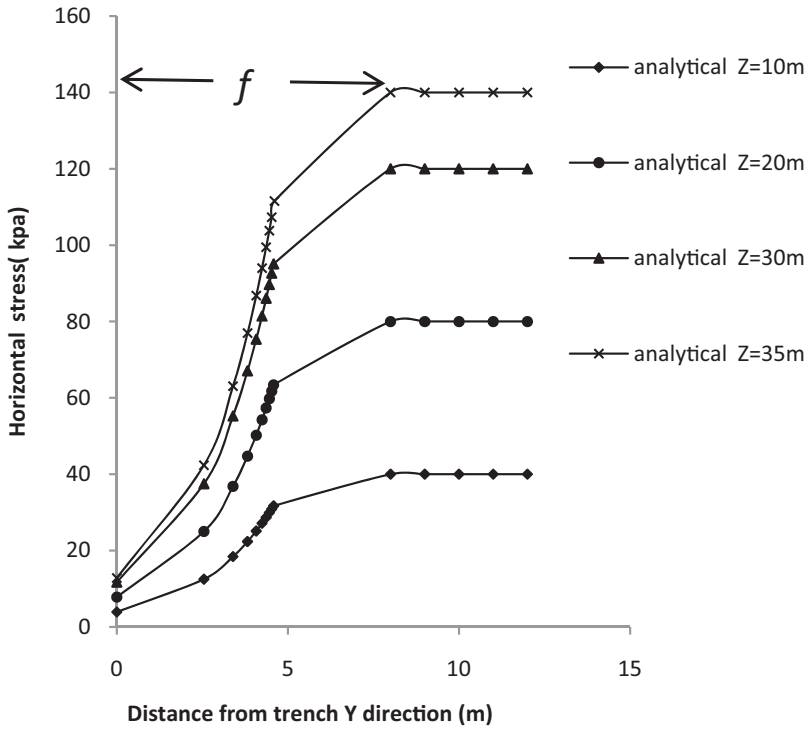

Fig. 5. Analytical results of unloading soil starting a distance f from the trench

Int. J. Geomech., 2017, 17(10): 04017081

Both variables $q/\cos\alpha$ and τ_A will be expressed in terms of σ'_1. As previously explained in this section, $q/\cos\alpha = \sigma'_1$, and under the proposed hypotheses at the arc ends, the following are obtained:

$$\begin{matrix} \alpha = \varphi \\ p = q \\ \tau_{A,B} = q\ \sin\alpha \end{matrix} \Rightarrow \tau_{A,C} = \frac{p}{\cos\varphi}\sin\varphi\ \cos\varphi \Rightarrow 2\tau_{A,C} = \sigma'_1\ \sin 2\varphi \tag{9}$$

Eq. (8) must be written differently after simplification by $L\,dz$ as

$$\frac{d\sigma'_1}{dz} + \frac{\sin 2\varphi}{L}\sigma'_1 - \gamma = 0 \tag{10}$$

Solving this differential equation, the following is obtained:

$$\sigma'_1 = \frac{\gamma L}{\sin(2\varphi)}\left(1 - e^{-\sin(2\varphi)\frac{z}{L}}\right) \tag{11}$$

Horizontal Arching

Horizontal arch in the x,y-plane during trench excavation releases a block of land laterally supported by the vertical arch effect. To describe the soil discharge function under the influence of horizontal arching, vault equilibrium in Eq. (10) was adapted such that in the y direction (σ'_3) the force of the weight of the arc was eliminated to obtain the following:

$$\frac{d\sigma'_3}{dy} + \frac{\sin 2\varphi}{L}\sigma'_3 = 0 \tag{12}$$

The solution of this equation is

$$\sigma'_3 = Ae^{\frac{-\sin(2\varphi)y}{L}}\ (A = \text{constant}) \tag{13}$$

This function describes the variation of the horizontal stress according to the distance y from the soil at rest to the trench sidewall (Fig. 4). In this case, the two boundary conditions are considered as follows:

- $y = 0 \Rightarrow \sigma'_3 = \gamma' z K_0$ $[\gamma' = \gamma_{sat} - \gamma_w$ unit weight $(= 1)$ the soil is not disturbed by trenching]. To determine the constant A, the following equation must be solved:

$$\sigma'_3 = Ae^{\frac{-\sin(2\varphi)0}{L}} = \gamma' z k_0 so\ A = \gamma' z k_0$$

$$\sigma'_3 = \gamma' z k_0 e^{\frac{-\sin(2\varphi)y}{L}} \tag{14}$$

- $y = f \Rightarrow \sigma'_3 = \gamma'_s z$ (f: the distance between the soil at rest and the trench sidewall; γ'_s: mud density underwater). To determine f, the distance of disturbed soil starting from the trench sidewall, the following equation must be solved:

$$\gamma' z k_0 e^{\frac{-\sin(2\varphi)f}{L}} = \gamma'_s z$$

$$f = \ln\left(\frac{\gamma' k_0}{\gamma'_s}\right)\frac{L}{\sin(2\varphi)} \tag{15}$$

The horizontal distance of the disturbed soil zone (Fig. 4) affected by the excavation depends on different parameters: friction angle, soil density, slurry density, and the coefficient of lateral earth pressure at rest. As highlighted by Ng and Yan (1999), there is a significant reduction of the lateral pressure behind the sidewall under the

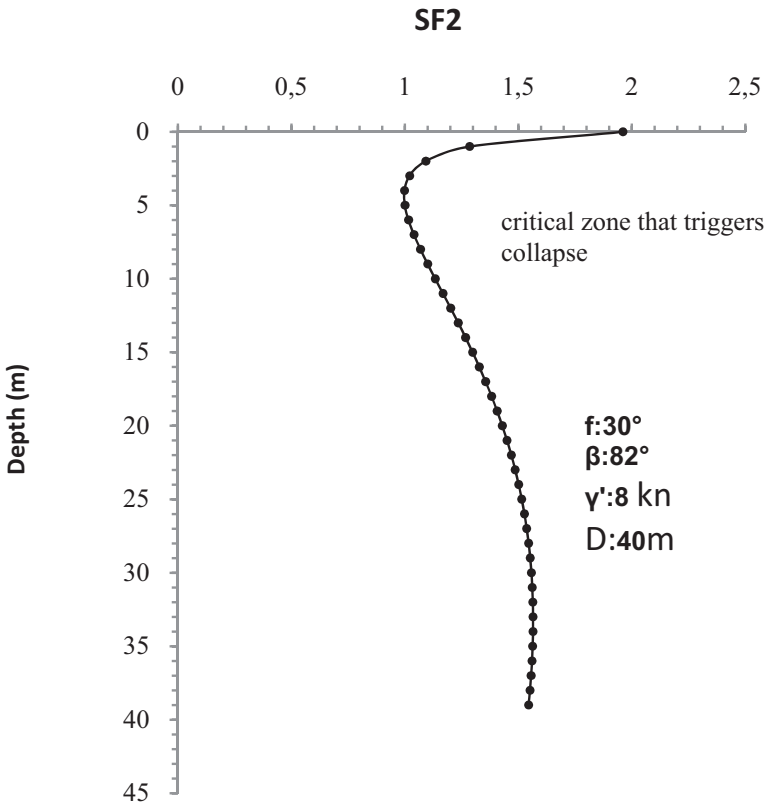

Fig. 7. Variations of the safety factor SF2 according to depth z

Int. J. Geomech., 2017, 17(10): 04017081

exponential influence of soil unloading starting from the trench sidewall. The example is a trench panel 3 m wide and 40 m deep in the soil layer that has the following features: γ of 18 kN/m^3, φ of 30°, c of 0, k_0 of 0.5, and γ_s of 11 kN/m^3 showing the variation of $\sigma_3^{'}$ for different depths depending on the distance y from the trench panel (Fig. 5). Analytical coordinates of points represented graphically is y; $\gamma' z k_0 e^{-\sin(2\varphi)y/L}$.

Interaction between Horizontal and Vertical Arching for Overall Stability

Downward load transfer mechanisms interact with horizontal arching through the sliding surface when the soil presents a limit equilibrium state as shown (Fig. 6) and by Li et al. (2011) and Piaskowski and Kowalewski (1965). The first consideration must be the variation of the vertical stress versus depth z proposed in function [Eq. (11)] and the sliding plane surface that gives the greatest thrust when inclined relative to the horizontal by angle β. In this case, $\mathrm{tg}(\beta) = D/f$ gives the largest contact surface, and hence, the largest horizontal thrust stress.

P_s is the horizontal component of soil reaction on the sliding surface and is expressed as follows:

$$\sigma_1' = F\cos(\beta - \varphi)$$
$$P_s = F\sin(\beta - \varphi)$$
$$P_s = \sigma_1' \mathrm{tg}(\beta - \varphi) \tag{16}$$

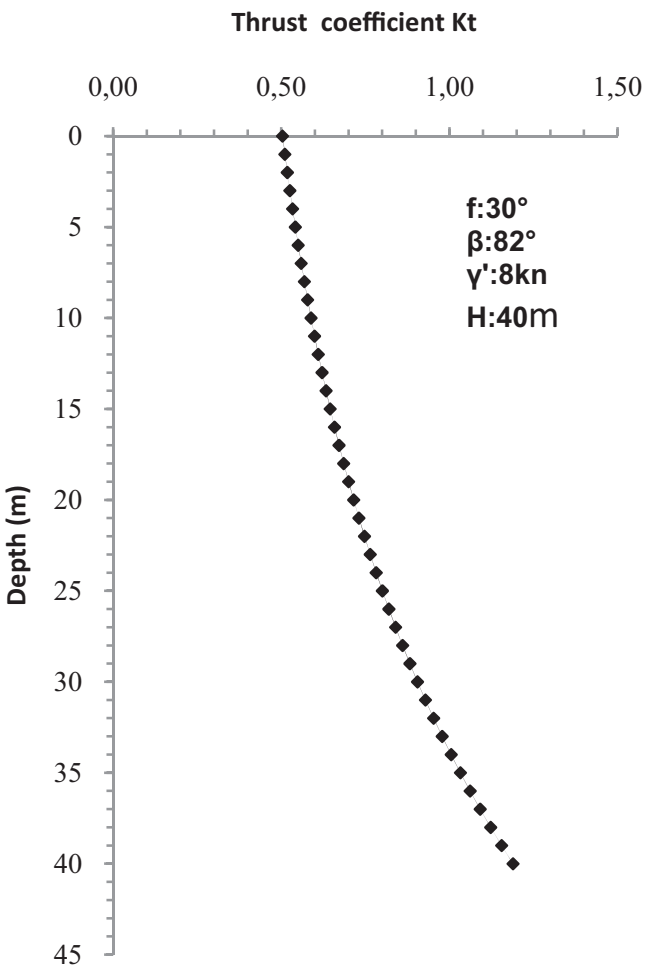

Fig. 8. Variations of pressure coefficient K_t

F is the resultant of frictional stress on the sliding plane inclined by angle φ. Overall trench stability leads to stabilized volume (V) (Figs. 1 and 6) through a safety factor that takes into consideration the balance between the two forces.

$$F_d = \frac{1}{\sin\beta}\int_0^{D/\sin\beta} P_s dz \quad (F_d\text{: destabilizing force})$$
$$F_s = \int_0^{D} \gamma_s z\, dz \quad (F_s\text{: stabilizing force}) \tag{17}$$

Under these conditions, trench stabilization depends on safety factor SF1 that should be greater than 1, thus

$$\mathrm{SF1} = \frac{F_s}{F_d} > 1 \ (\mathrm{SF1}\text{: overall safety factor})$$

Interaction between Horizontal and Vertical Arching for Interface (Local) Stability

The general stability of the trench is reflected by a safety factor higher than 1, but nothing prevents the collapse of the trench by interface instability. Trench interface is influenced by two types of active stress: P_s applied to the sliding surface and $\sigma_1' k_a$, the natural active soil pressure applied directly on the interface. However, horizontal stress, P_s, decreases under the xy arching effect; thus, lateral pressure on the trench interface triggered by P_s is exponentially reduced from the sliding plane to the trench interface as follows:

$$\sigma_3' = P_s e^{\frac{-\sin(2\varphi)y}{L}} + \sigma_1' k_a \ (\sigma_3'\text{: active stress applied on the trench interface}) \tag{18}$$

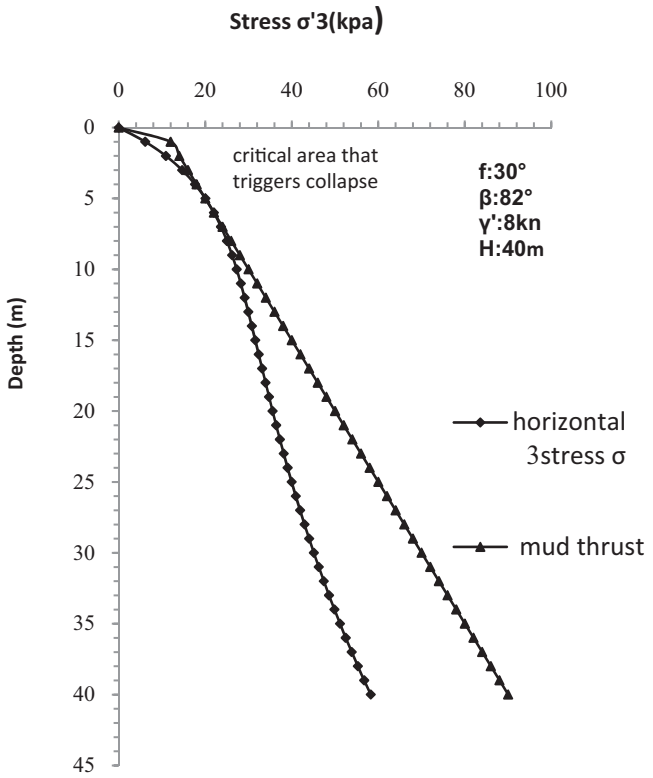

Fig. 9. Variations of σ_3' stress versus mud pressure

The active stress is applied on the trench interface y and z coordinates; however, $y = (D - z)\text{tg}(\pi/2 - \beta)$ is used to write the formula as a function of z as follows:

$$\sigma'_3 = \sigma'_1\left[\text{tg}(\beta - \varphi)e^{\frac{-\sin(2\varphi)(D-z)\text{tg}\left(\frac{\pi}{2}-\beta\right)}{L}} + k_a\right] \tag{19}$$

This function leads to propose

$$K_t = \left[\text{tg}(\beta - \varphi)e^{\frac{-\sin(2\varphi)(D-z)\text{tg}\left(\frac{\pi}{2}-\beta\right)}{L}} + k_a\right]$$
$$\sigma'_3 = K_t\sigma'_1 \tag{20}$$

where $k_a = \text{tg}2(\pi/4 - \varphi/2)$ = Rankine's pressure coefficient; and K_t = lateral pressure coefficient on the interface, which depends on several parameters (φ, L, and β) and also varies depending on depth, z; this coefficient is unlike the results found by Piaskowski and Kowalewski (1965) [Eq. (19)]. To stabilize interface at any points of trench depth, it is necessary that lateral active pressure is less than passive mud pressure.

$$\text{SF2} = \frac{\gamma'_s z}{K_t\sigma'_1} \geq 1 \text{ (SF2: interface safety factor)}$$

Safety Factors of Trench Stability

Trench stability must be checked using two safety factors. The first safety factor ensures overall stability and prevents sliding collapse. The second safety factor provides pressure equilibrium of each interface point in the two sides. Therefore, the total stability of the trench is satisfied when SF1 > 1 and SF2 >1 for each interface point.

$$\text{SF1} = \frac{\int_0^D \gamma'_s z dz}{\frac{1}{\sin\beta}\int_0^{D/\sin\beta} P_s dz} = \frac{0.5\gamma'_s D^2}{\left\{\frac{\gamma' LD}{\sin\beta\sin(2\varphi)} + \frac{\gamma' L^2}{\sin(2\varphi)^2}\left[e^{-\sin(2\varphi)\frac{D}{L\sin\beta}} - 1\right]\right\}\frac{\text{tg}(\beta-\varphi)}{\sin\beta}} > 1 \tag{21}$$

$$\text{SF2} = \frac{\gamma'_s z}{K_t\sigma'_1} = \frac{\gamma'_s z}{\left[\text{tg}(\beta - \varphi)e^{\frac{-\sin(2\varphi)(D-z)\text{tg}\left(\frac{\pi}{2}-\beta\right)}{L}} + \text{tg}^2\left(\frac{\pi}{4} - \frac{\varphi}{2}\right)\right]\frac{\gamma' L}{\sin(2\varphi)}(1 - e^{-\sin(2\varphi)\frac{z}{L}})} > 1 \tag{22}$$

Assumed Application Examples

The example of a trench in a soil layer has the following features: γ of 18 kN/m^3, φ of 30°, and c of 0; filled with slurry of density γ of 11 kN/m^3; trench dimensions, L of 3 m and D of 40 m; and water table level at the ground surface. The aim of the study was to show the variations of SF2, K_t, and σ'_3 according to depth z. The results indicate that SF2 tended toward a limit value when the trench depth exceeded 25 m, and it took a minimum value at 7-m depth (i.e., 1/4D). Furthermore, the critical area that triggered trench collapse was characterized by the lowest safety factor, which was located between 5 and 10 m deep, as shown in Fig. 7. The trench sidewall was influenced by several involved stresses that explain such behavior for SF2. The stabilization stresses varied linearly along the depth of the lateral surface. However, the earth pressures developed more rapidly because the vault effect was low for the small depths, creating a critical zone triggering trench collapse. Furthermore, the increase in earth stresses became weaker because the strong intervention of the arching effect in the greater depths favored stability.

The lateral thrust coefficient on the sidewall interface, K_t, varies between 0.5 m at top and 1.1 m at trench toe (Fig. 8). This factor took the k_a value at the soil surface and then gradually increased along the interface until the maximum value reached at the toe (Xiao et al. 2015); this effect is due to the influence of horizontal stress P_s resulting with the sliding plane initiation. In addition, the

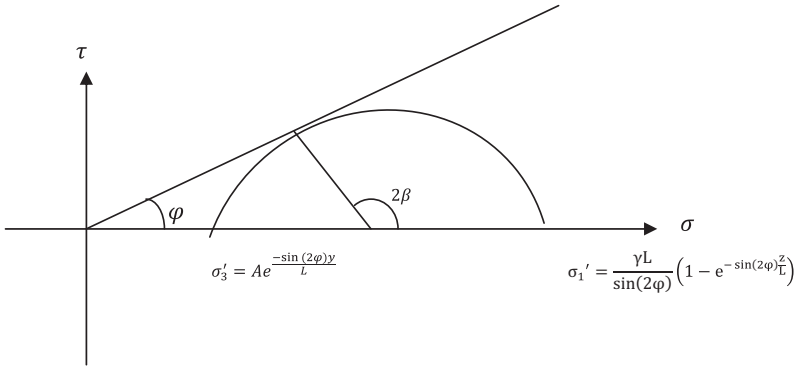

Fig. 10. Location of plastic points behind the trench interface

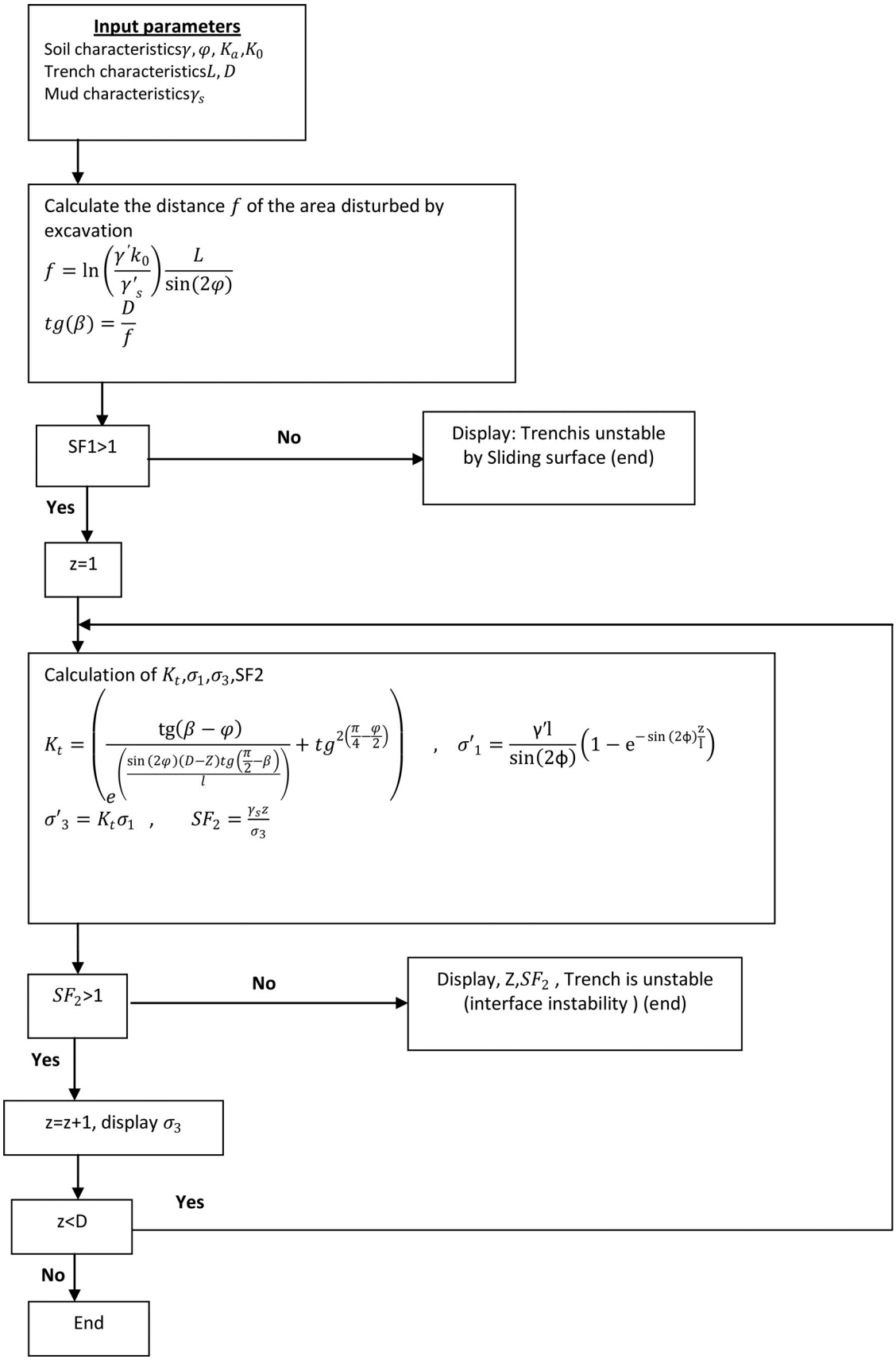

Fig. 11. Algorithm of the analytical approach

distance separating the interface from the sliding surface decreased linearly until the bottom of the sidewall unloaded P_s differently according to z levels under the xy arching effect, which led to K_t to becoming a variable term of z depth.

The variation of σ'_3 stress and mud pressure on the trench sidewalls is very essential to delimit the areas that can cause disequilibrium of the interface of the trench lateral surface and subsequently a collapse. The level of the water table was folded at the lower level because of excavation, and as seen in Fig. 9, both pressure curves are tangent between 5 and 10 m deep and diverge when the depth exceeds 10 m. This means that the points of the interface in this area present a limit equilibrium that can trigger a collapse at any time.

Overall, the stability of the trench versus the sliding risk is ensured by the safety factor SF1, but it is possible to study the variation of σ'_1 in terms of z [Eq. (11)] and the variation of σ'_3 according to y to locate plastic points in the x,z-plane, which can cause a sliding surface through Mohr's circle and the curve rupture shown in Fig. 10. To facilitate the task, the proposed algorithm of this approach that gives the values of SF1, SF2, the distance value of the area disturbed by excavation, earth pressure for each depth z, and location of the critical area that triggers collapse is presented in Fig. 11.

FE Analyses and Field Measurements

An experimental model and FE analyses using *PLAXIS 3D* of a slurry-wall panel are carried out to compare the ground stress around trenches against the analytical solution. For this case, a rectangular section (2.8 m long and 40 m deep) of the trench panel was adopted in sedimentary soil located in the region of Hong Kong. This excavation has been the subject of analysis performed by a geotechnical team led by Lei at the University of Science and Technology of Hong Kong in 1998 (Lei et al. 1999). The trench behavior during excavation and lateral earth pressures on the trench sidewall immediately before and after concreting were observed and measured with instrumentation. In this part of the work, 3D coupled numerical calculations were developed using the hardening-soil model more suitable to simulate the behavior of the slurry-wall trench in cohesionless soil (Tsai and Chang 1996). Calculation assumptions, modeling steps, numerical results, and in situ measures are presented.

Description of the Trench Site

The trench site was located in Kowloon, in the extremities of the Hong Kong region, to the east of the runway of the former Kai Tak International Airport, surrounded by the Central Laboratory of Public Works and Kowloon Bay. The site was located in a built-up area reclaimed from the sea, and the soil surface was approximately 4.50 m above sea level. The level of the water table was 3 m below the ground surface. The mechanical properties of the soil were evaluated mainly by standard penetration tests (SPTS), and the geotechnical conditions of the entire Kowloon area were interpolated from different testing points. The properties are shown in Table 1 from the work performed by Lei et al. (1999).

Modeling and Calculation Assumptions

To verify the validity of the analytical approach proposed in this study, a 3D numerical model of a deep planar excavation (width, $W = 1$ m; length, $L = 3$ m; and depth, $D = 40$ m) using FEM carried out for comparing the numerical and analytical results of stresses developed in the soil around the trench. The environment and soil conditions are idealized (uniform stratification, stiffness, and K_0 are uniform in all layers) (Gourvenec and Powrie 1999). To generate the initial stress conditions, it was assumed that the soil remained drained with a constant Poisson's ratio, ν, of 0.5 and the lateral pressure coefficient, K_0, of 0.5. To minimize the effects of boundary conditions on the calculation results and allow any mechanism to occur in all three directions, the project was modeled in a 3D space 75 m long, 16 m wide, and 50 m deep (defined as the calculation domain), and the separation distance from the trench to the boundary conditions is 30 m. The vertical boundaries were fixed on roller supports to limit normal motion to the boundary line and the base of the calculation domain was set to prevent movement in all directions. Meshes were discredited in more than 20,000 elements, taking into account the effect of mesh refinement on the accuracy of the calculation, and the excavation was modeled by removing the elements within the trench area and simultaneously applying normal hydrostatic pressures to the exposed surfaces. The hardening-soil model is the most suitable to simulate the behavior of the slurry-wall trench in cohesionless soil because the advantage of hardening soil over the Mohr-Coulomb model is not only the use of a hyperbolic stress-strain curve instead of a bilinear curve but also the control of stress-

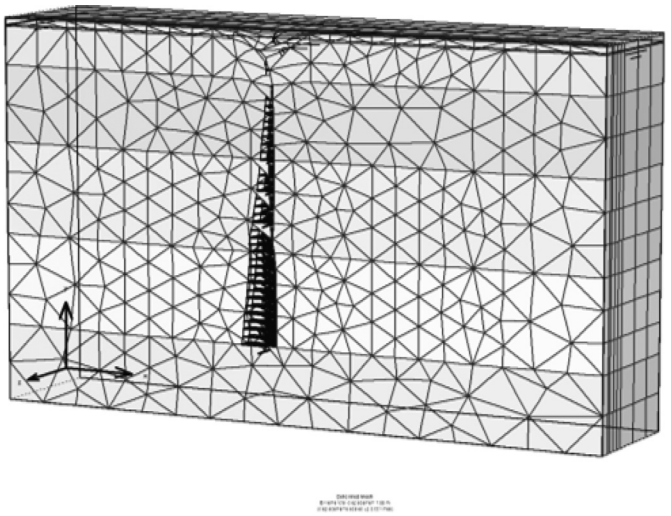

Fig. 12. Presentation of 3D mesh geometry

Table 1. Mechanical Properties of Soils

Soil layer	Higher level (m)	Lower level (m)	γ (kN/m^3)	c' (kPa)	φ' (degrees)	G (MPa)
Backfill	+4.50	−1.50	18.0	0,0	28.0	12
Marine depot	−1.50	−11.50	18.0	0,0	28.0	12
Quaternary alluvium	−11.50	−23.50	20.0	0,0	33.0	10–32
Altered granite	−23.50	−35.50	20.0	0,0	39.0	>32
Heath granite	−35.50	Unknown	20.0	0,0	45.0	—

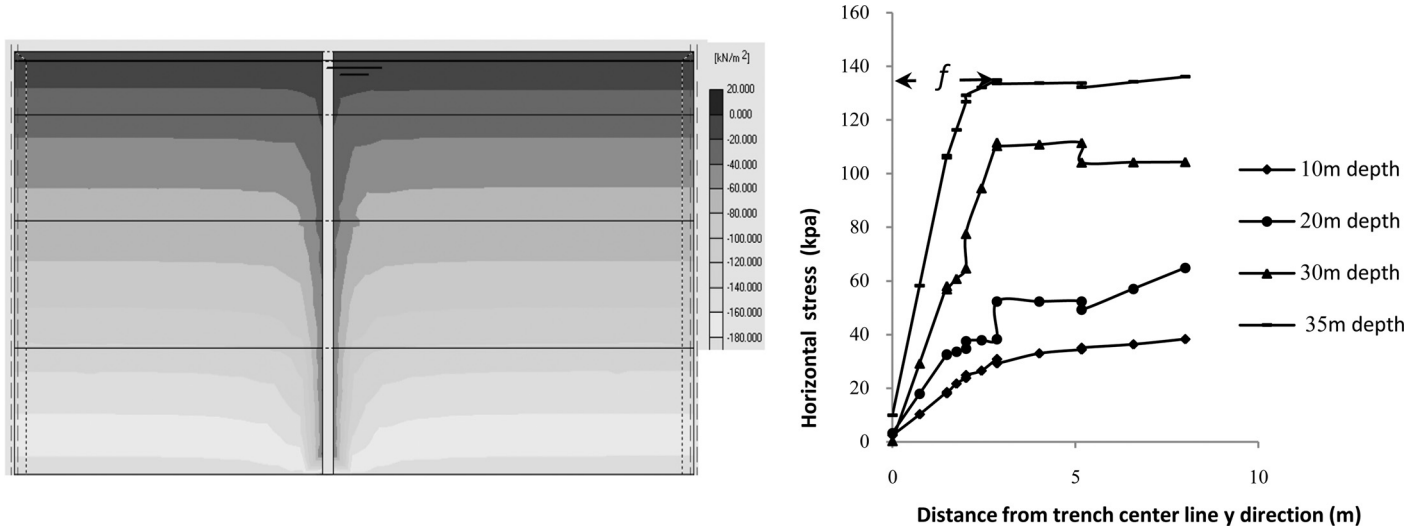

Fig. 13. Earth pressure variations for different depths in the *y* direction

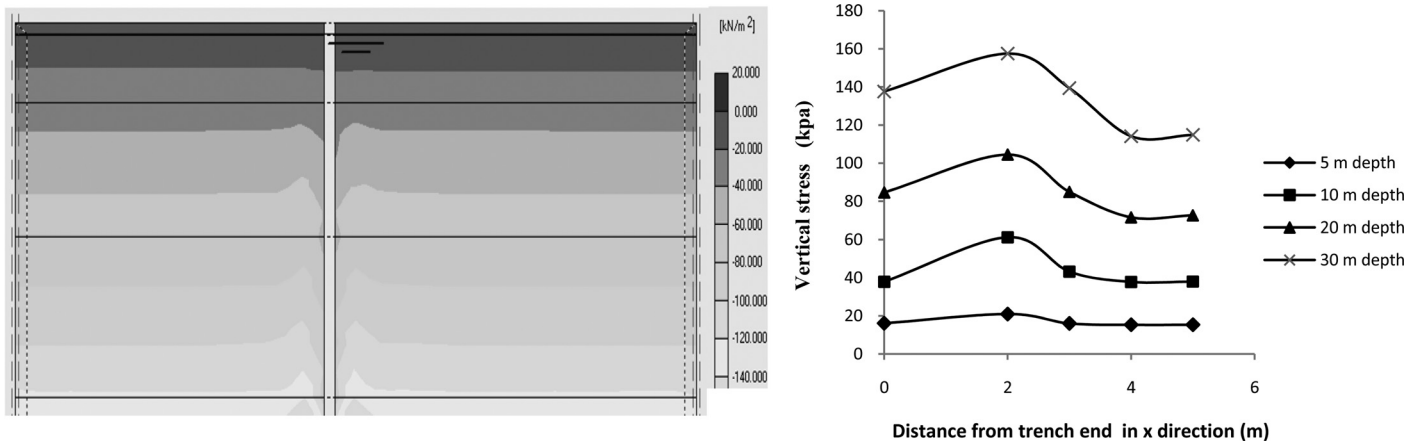

Fig. 14. Reloading soil in the *x* direction in the longitudinal direction

level dependency. For real soil, the different modules of stiffness depend on the stress level (Yonggang et al. 2011). Some parameters of the present hardening model coincided with those of the classical nonhardening Mohr-Coulomb model: failure parameters $\varphi, c,$ and ψ (dilatancy angle). In addition, the basic parameters for soil stiffness were used. E_{50}^{ref} refers to the secant stiffness in a standard drained triaxial test, $E_{\text{oed}}^{\text{ref}}$ refers to the tangent stiffness for primary oedometer loading, and m is the power for the stress-level dependency of stiffness. The set of parameters was completed by the following advanced parameters: E_{ur}^{ref} is unloading/reloading stiffness; ν_{ur} is Poisson's ratio for unloading-reloading; P^{ref} is the reference stress for stiffness; and K_0^{NC} is the K_0 value for normal consolidation. Experimental data on m, E_{50}, and E_{oed} for granular soil were given in Schanz and Vermeer (1998).

The water table level was 3 m from the soil surface. The trench was symmetric in the longitudinal direction, so only one-half the thickness needed to be modeled (Fig. 12).

The 3D mesh generation model was extended 16.0 m in the x direction to allow for any possible mechanism to occur in the x direction and to avoid any influence from the boundaries. Five planes were entered, a front plane at $x = 0.0$ m, Plane A at $x = -0.6$ m, Plane B at $x = -2$ m, Plane C at $x = -7$ m, and a rear plane at $x = -10.0$ m. Because the largest gradient of displacement in the x direction occurs around Plane A, a local mesh refinement was applied around Plane A. Mud with a unit weight of 11.5 kN/m^3 was simulated by means of an artificial water pressure that increased linearly with depth; this pressure replaced the original water pressure inside the excavation. All calculation phases were defined as plastic calculations of the load-advancement ultimate level type using staged construction as the loading input.

Results and Discussion

The results provided by the numerical model show the soil behavior through the variation of stress fields of σ_1' and σ_3' behind the sidewall trench in the x,z- and y,z-planes. *PLAXIS 3D* results confirmed that the unloading function of σ_3' took an exponential form, creating a disturbed area, f, of 3 m in the y,z-plane along the centerline perpendicular to the trench (i.e., along the y-axis) (Fig. 13) and showed σ_3' distributions for a 1-m-wide trench with various depths and

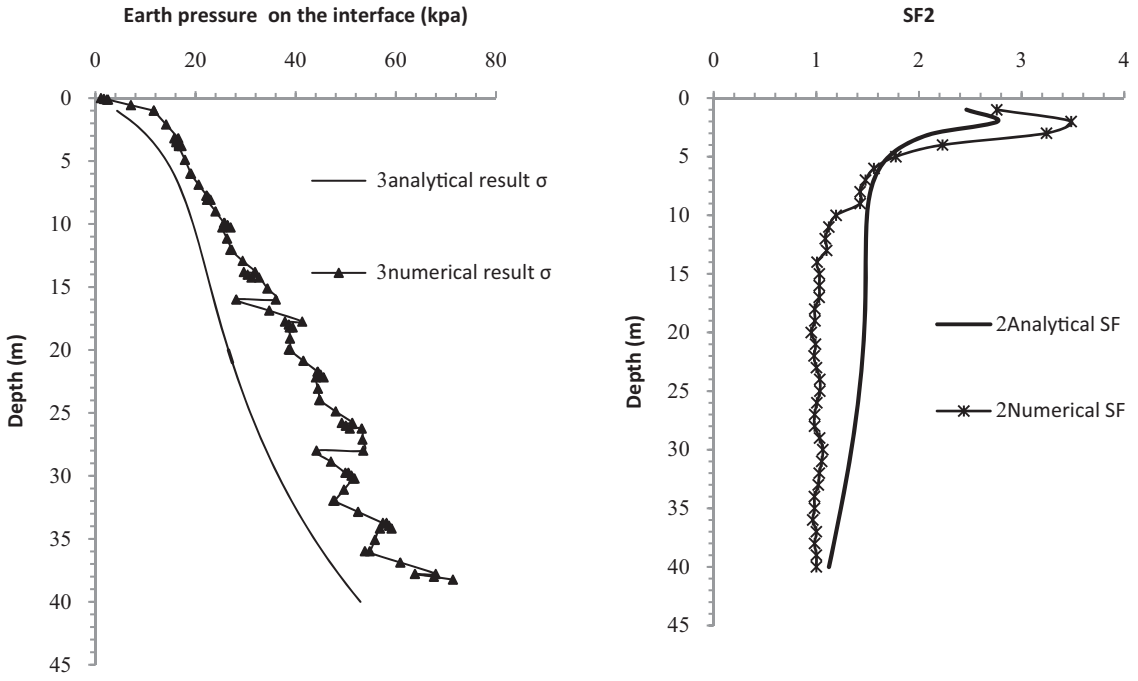

Fig. 15. Numerical and analytical results of earth pressure on the interface

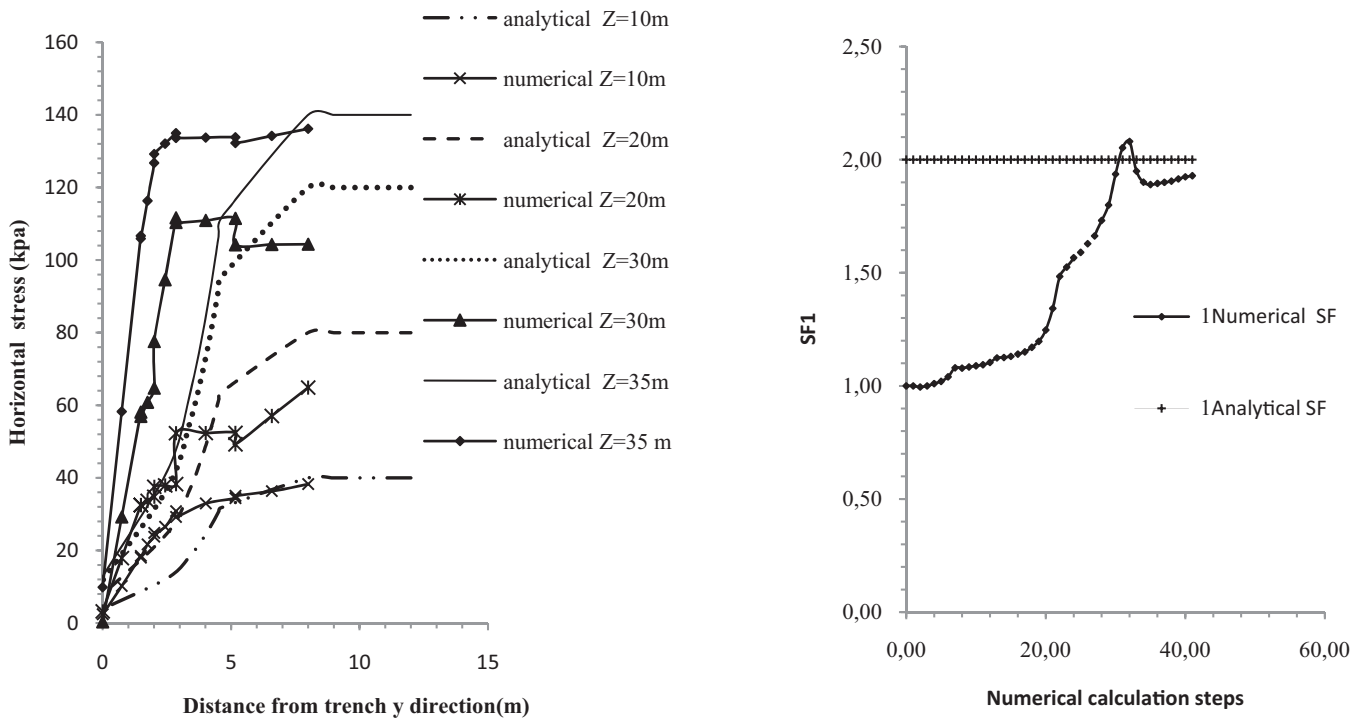

Fig. 16. Variation of horizontal stress behind the wall

aspect ratios, respectively. Partial recovery of total normal horizontal stresses occurred during the construction of an adjacent panel under the effect of the horizontal arching mechanism that plays a key role in redistributing total normal horizontal stress from the center to the interface. The redistribution of horizontal load was achieved via the shear stress (τ_{xz}). Stress variation was the smallest at the center but increased in magnitude toward the sidewall. Furthermore, σ_3' were shed vertically downward beneath the toe via the sliding surface and shear stress, τ.

In the x,z-plane the soil was loaded onto the longitudinal ends of the trench because of the vertical arch effect, and a variation of this load along the x direction under the effect of the horizontal vault effect was confirmed (Fig. 14). The reloading of soil at panel ends in the x direction is attributed to the fact that a downward transfer mechanism, influenced by the vertical arching effect, leads to an increase in σ_1' at the ends and a decrease along the centerline perpendicular to the trench. These two mechanisms act simultaneously and result in an average reduction of horizontal stress directly behind the wall above the

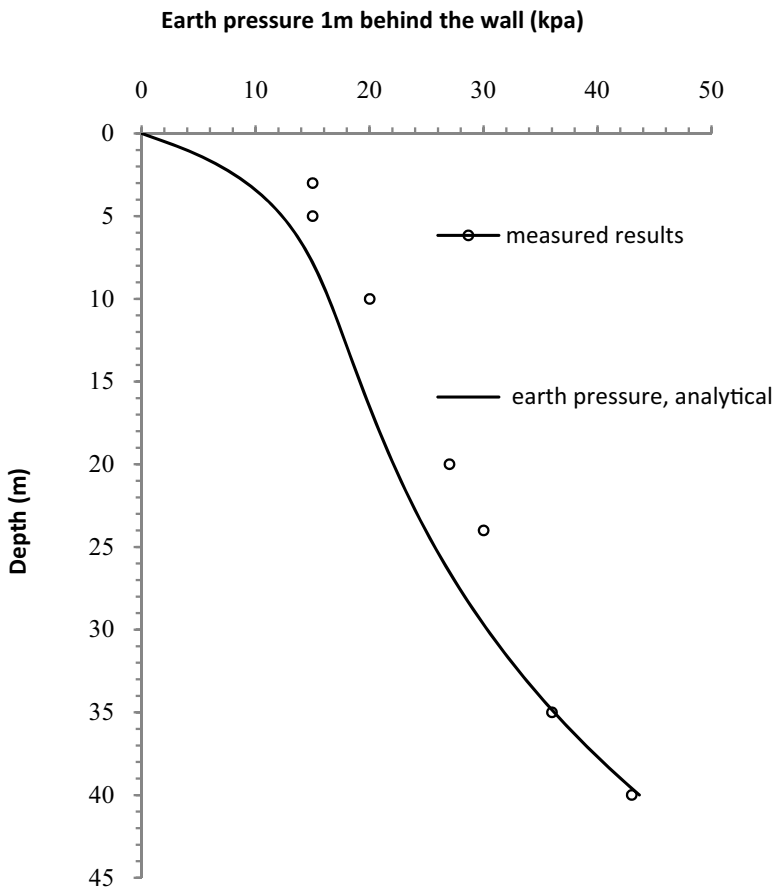

Fig. 17. Comparisons between calculated and field measurements, σ_3'

toe but an increase of vertical stress in neighboring soil beyond the wall in the longitudinal direction and below the toe of the wall.

Comparisons between Analytical Solutions and FE Analyses

The results given by the analytical method and those from the numerical 3D modeling were compared with regard to the lateral earth pressure on the interface and the safety factors (Fig. 15). The horizontal stresses at the soil-mud interface given by FE analyses were slightly higher than the analytic results because of misjudgments of K_0. Furthermore, the difference is attributed to 3D analysis that overestimated the amount of downward load transfer as a result of the two coupled plane analyses by implicit FEM, which has a tendency to increase the stress in the ground. An acceptable difference was found between the numerical and analytical results concerning the stress values of horizontal push and SF2 in soil near the trench.

There is an exponential change in the horizontal stress in the y direction, which is easily explained by the formation of a vault that changes the horizontal earth pressure in the disturbed area. From the soil pressure at rest to the mud pressure described with the analytical function, $\sigma_y = \gamma' z k_0 e^{-\sin(2\varphi)y/l}$, the variation depending on the depth z is shown in Fig. 16. It was determined that 3D analysis overestimates the stress attributed to the downward load transfer mechanism (Tsai 1997) and neglects the role of the vertical arch effect in the disturbed area. These errors led to a slight difference between the numerical and analytical results. Numerical results of the safety factor increased step by step until they reached the value of the analytical calculation of the overall safety factor, SF1, at the end of the excavation.

Comparisons with Field Measurements

Because of insufficient information for a detailed study, a general comparison was made between the calculated stress and some relevant field measurements data produced by Lei et al. (1999), to supported slurry trenches in the Kowloon, Hong Kong, region. The lateral pressures on the sidewall of the trench before concreting were observed and measured with instrumentation.

The proposed simplification in the calculation model for the value of K_0 and the stiffness of the soil may explain the differences between the calculated and measured results (Fig. 17). In the case studied, it is probable that the soil had a relatively high K_0, variable stiffness as a function of depth (increasing stiffness with depth), and a relatively greater stiffness at a great distance from the trench (Conti et al. 2012). Furthermore, some stress could result from the installation of guide walls or neighboring panels. Although there are differences between the calculated and measured results, it was found that the use of conservative material parameters, such as K_0 and E, the comparison suggests an upper limit to the set of adopted data.

Conclusion

An analytical solution was proposed using the effective stress analysis method for the description of the phenomenon of deep trench stability of slurry walls. Trench stability was governed by the contribution of the interaction between horizontal and vertical arching, creating a length f of the soil disturbance zone behind the sidewall and causing the formation of an inclined sliding surface from the horizontal axis in this area. Moreover, this approach defined a new

parameter, K_t, the interface pressure coefficient, that depends on several parameters: the trench length, friction angle, trench depth, and length of the disturbed area. Key parameters governing the stability of trench are the safety factors SF1 (general safety factors) and SF2 (interface safety factor); SF1 ensured overall stability and prevents sliding collapse, and SF2 provided pressure equilibrium for each interface point in the two sides. Qualitative consistence was obtained between the results from the proposed solution and the FE analyses by adopting an appropriate set of material parameters. The analytical approach developed in this article gave results comparable to those found by measurements for slurry-supported trenches in Kowloon, Hong Kong. Seeing that the measurement technique is used extensively in the urban areas, the authors look forward to improving the analytical approach by taking into account buildings near excavation sites and the cohesion effect on trench stability.

Notation

The following symbols are used in this paper:

c = cohesion angle of the soil;
ds = elementary surface of integration;
dx, dz, dy = differential distance in the x, y, and z direction, respectively;
f = disturbed soil distance from the trench sidewall;
K_0 = coefficient of lateral earth pressure at rest;
K_t = lateral pressure coefficient on the sidewall interface;
k_a = Rankine's pressure coefficient;
L, W, D = length, width, and depth of a trench;
P_h, P_v = horizontal and vertical total earth pressures;
P_s = horizontal component of soil reaction on the sliding surface;
p, q = stress applied to the elementary volume;
x, y, z = global Cartesian coordinate axes;
α = curvature angle at a point of an arc;
β = angle to the horizontal plane of the sliding surface;
γ_{sat} = saturated unit weight of soil;
γ_s, γ_w = unit weights of slurry and water;
γ_s', γ' = unit weights of slurry under water;
φ = friction angle of soil;
σ_x = horizontal stress applied at elementary volume of an arc;
$\sigma_1', \sigma_2', \sigma_3'$ = effective stress in the z, x, and y direction, respectively; and
τ_A, τ_C = shear stresses at the arc ends.

References

Carlos, E. G. T., and Theodoros, T. (2012). "Simulation of a corner slurry trench failure in clay." *Comput. Geotech.*, 45, 107–117.

Conti, R., De Sanctis, L., and Viggiani, G. M. B. (2012). "Numerical modelling of installation effects for diaphragm walls in sand." *Acta Geotech.*, 7(3), 219–237.

Fox, P. J. (2004). "Analytical solutions for stability of slurry trench." *J. Geotech. Geoenviron. Eng.*, 10.1061/(ASCE)1090-0241(2004)130:7(749), 749–758.

Gourvenec, S. M., and Powrie, W. (1999). "Three-dimensional finite element analysis of diaphragm wall installation." *Géotechnique*, 49(6), 801–823.

Han, C., Chen, J., Wang, J., and Xia, X. (2013). "2D and 3D stability analysis of slurry trench in frictional/cohesive soil." *J. Zhejiang Univ. Sci. A*, 14(2), 94–100.

Lei, G. H., Douglas, R., Ng, S. W. L., and Ng, C. W. W. (1999). "Observed performance of a short diaphragm wall panel." *Géotechnique*, 49(5), 681–694.

Lei, G. H., Sun, H. S., and Ng, C. W. W. (2014). "An approximate analytical solution for calculating ground surface settlements due to diaphragm walling." *Comput. Geotech.*, 61, 108–115.

Li, S. J., Chen, J., and Feng, X. T. (2011). "Analytic solution to soil arching effect and its application based on interaction of slope soil and piles." *Mater. Res. Innovations J.*, 15(S1).

Mohamed, A. (2015). "Effect of groundwater table rising and slurry reduction during diaphragm wall trenching on stability of adjacent piles." *IOP Conference Series: Earth and Environmental Science*, Vol. 26, Institute of Physics, Bristol, U.K, 012012.

Ng, C. W. W., and Yan, R. W. M. (1999). "Three-dimensional modeling of a diaphragm wall construction sequence." *Géotechnique*, 49(6), 825–834.

Piaskowski, A., and Kowalewski, Z. (1965). "Applications of thixotropic clay suspensions for stability of vertical sides of deep trenches without strutting." *Proc., 6th Int. Conf. on Soil Mechanics and Foundation Engineering*, University of Toronto Press, Toronto, 526–529.

PLAXIS 3D [Computer software]. Plaxis bv, Delft, Netherlands.

Schanz, T., and Vermeer, P. A. (1998). "On the stiffness of sands." *Géotechnique Pre-failure Deformation Behaviour of Geomaterials*, Vol. 48, Thomas Telford, London. 383–387.

Tsai, J. S. (1997). "Stability of weak sublayers in a slurry supported trench." *Can. Geotech. J.*, 34(2), 189–196.

Tsai, J. S., and Chang, J. C. (1996). "Three-dimensional stability analysis for slurry-filled trench wall in cohesionless soil." *Can. Geotech. J.*, 33(5).

Xiao, F. J., Shu, T. L., and Xiao, J. Z. (2015). "Stability of three-dimensional slurry trenches with inclined ground surface: A theoretical study." *Adv. Mater. Sci. Eng.*, 2015, 362160.

Yonggang, X., Zilong, W., Guannan, Z., and Yuyong, S. (2011). "Analysis of stability of slurry trench sides of diaphragm wall based on construction parameters." *Chin. J. Rock Mech. Eng.*, 30(2), 3464–3470.